Abundance Analysis of the Pulsating Primary Component of the Algol-Type System AS Eridani * †

Shin-ya Narusawa
Nishi-Harima Astronomical Observatory, Center for Astronomy, University of Hyogo
Sayo-cho, Hyogo 679-5313
narusawa@nhao.jp

Abstract

We have carried out an abundance analysis of the pulsating primary component of an Algol-type binary system AS Eridani. The spectral data obtained with the Subaru/HDS were used and the abundances of six elements (Mg, Si, Ca, Ti, Cr and Fe) were determined relative to an A3 V spectroscopic standard star α PsA. The under-abundance of iron (-0.66 dex) has been established. Other elements, Mg through Cr are also under-abundant (~ -0.4 dex). No difference in abundances at different orbital phases has been found. The physical relation between the metallicities and the pulsational characteristics is discussed.

1. Introduction

In eclipsing binary systems, physical parameters (e.g. mass, radius, luminosity, etc.) can be determined by light curve and radial velocity analysis. On the other hand, asteroseismology is used for study of stellar inner structures. Hence eclipsing binaries which have a pulsating component(s) are important objects for astrophysics. Tempesti (1971) reported that a primary component of an Algol-type system AB Cassiopeiae is a pulsator. This was the first discovery that the component shows a pulsation in eclipsing binaries. After Ohshima et al. (1998, 2001) detected a non-radial pulsation (NRP) in the primary component of an Algol-type binary system RZ Cassiopeiae (A3 V+K0 IV, $P_{\rm orb} = 1.1953$ day, called "RZ Cas-p" hereafter), a number of surveys have been carried out and oscillations were discovered in many components of eclipsing binary systems (e.g. Derekas et al. 2009, Dimitrov et al. 2010, Damiani et al. 2010, Hambsch et al. 2010 , Southworth et al. 2011, Liakos et al. 2012).

Most of pulsating components of the Algol-type binary are classified into δ Sct variables.

---

* Based on data collected at Subaru Telescope, which is operated by the National Astronomical Observatory of Japan.

† In part on data collected at Okayama Astrophysical Observatory and obtained from the SMOKA, which is operated by the Astronomy Data Center, National Astronomical Observatory of Japan.

This type stars are mostly variables of A-F spectral type located in the Cepheid instability strip and the period ranges are limited to between $\sim$ 30 min and $\sim$ 6 hr (Breger 2000). Soydugan et al. (2006) performed statistical study on eclipsing binary systems having pulsational components located in the δ Sct region. Zhou (2010) made a catalogue of more than 370 pulsating components in binary/multiple stellar systems. Total 60 δ Sct components of 146 eclipsing binaries are listed in the catalogue. Liakos et al. (2012) made a catalogue of 74 close binaries including a δ Sct companion. Moreover, Uytterhoeven et al. (2011) analysed the *Kepler* light curves of 750 A-F type stars and found that 206 stars are δ Sct pulsating stars, seven of which are component stars of eclipsing binaries. Since many pulsators have been found in the primary components of the Algol-type binaries, Mkrtichian et al. (2002, 2003, 2005, 2007) introduced a new class of pulsating stars, oscillating EA (oEA, Mkrtichian et al. 2002) . According to their definition, the new group consists of pulsating mass-accreting main sequence stars of spectral type A-F in semi-detached Algol-type systems. This type stars have much similar pulsating characteristics as δ Sct stars but have experienced a quite different evolution process due to the mass-transfer. About 50 stars of 60 δ Sct pulsators in Zhou's catalogue are marked as oEA type stars. The period range of oEA is almost the same as that of the δ Sct type stars. On the other hand, another short period type – rapidly oscillating Ap (roAp) – stars occupy the same region with the δ Sct (and oEA) stars on the HR diagram. The typical pulsating period of roAp stars is 4-15 min (Kurtz 1990). The pulsation of δ Sct type is driven by the κ-mechanism in the He II, while that of the roAp type is driven by the κ-mechanism of the H I. The excitation mechanisms of δ Sct type and roAp type are different, however the periods are overlapped each other. In fact, the shortest period of δ Sct-type is 11-12 min in KIC 4840675 (Balona et al. 2012), while the longest period of roAp star is 23.6 min in HD 177765 (Alentiev et al. 2012).

The both A3 V primary components of the Algol system RZ Cas and AS Eridani are short period non-radial pulsators and they are classified into the oEA stars. However, the periods of RZ Cas-p and the primary component of AS Eri ($P_{\rm pul} \sim 20$ min, called "AS Eri-p" hereafter) are around at the border between δ Sct-type and roAp stars. On the other hand, Liakos et al. (2012) derived an empirical relation between orbital and pulsational periods of δ Sct components in eclipsing binaries. According to their equation, pulsation periods are expected to 44 ± 5 min and 73 ± 11 min for RZ Cas-p and AS Eri-p, respectively. However, observational pulsation periods do not agree with the expected values. To study common pulsational mechanism between RZ Cas-p and AS Eri-p is important because there is a possibility that these two stars are unusual type of δ Sct-type (and/or oEA).

We started with an abundance analysis to seek the similarity between RZ Cas-p and AS Eri-p. Narusawa et al. 2006a (hereafter referred to as Paper I) found that RZ Cas-p shows similar characteristics of λ Boötis-type stars. This type stars are Population I, A- to F-type stars, in which heavier elements are underabundant relative to the Sun, whereas the light elements have near-solar abundance (see, e.g., review by Paunzen 2004).

Spectroscopic observation of AS Eri was carried out by Popper (1973) and he reported that AS Eri is not an Am star. However, there has been no detailed abundance analysis of this star up to now. In this paper, we report result of abundance analysis in AS Eri-p. AS Eri (A3 V+K0 III, $P_{\rm orb} = 2.6642$ day) was discovered by Hoffmeister (1934). Gamarova et al. (2000) first detected the short-period oscillations in the primary component and reported that the dominant frequency is 59.03 cd^{-1} ($P_{\rm pul} = 24.39$ min). Mkrtichian et al. (2004) carried out a multi-site photometric campaign in 2000 and revealed a pulsational behavior with three frequencies of $f_1 = 59.03116$ cd^{-1}, $f_2 = 62.5631$ cd^{-1} and $f_3 = 61.6743$ cd^{-1}. They suggested that the sectoral (l, m, n) = (1, 1, 5) or (2, 2, 5) and (l, m, n) = (2, -2, 6) modes were identified for two oscillation frequencies f_1 and f_2 modes, respectively.

2. Observational Data

AS Eri is a double-lined spectroscopic binary (Popper 1973), and the secondary component (called "AS Eri-s" hereafter)'s absorption lines are distinct in the spectrum. The intensity ratios of AS Eri-s to total intensity are 18 percent in y-band and 11 percent in b-band, respectively (van Hamme and Wilson 1984). To determine the surface abundances of primary component, we subtracted the contribution of AS Eri-s from the observed spectrum. In order to avoid an overlap between primary's line and secondary's line, we used spectra obtained at out of eclipses when the two components show different doppler shifts. We obtained the spectral data of A3 V and K0 III stars as the reference stars of primary and secondary, respectively.

Since we did not have any information about abundances of AS Eri-p, we conducted two procedures, a preliminary analysis and a detailed analysis. In the preliminary analysis, we used medium-dispersion spectral data for a rough estimate of the abundances. In the next step, high-dispersion spectra were used for their determination. Data of AS Eri and reference stars are shown in table 1.

2.1. Data for Preliminary Analysis

For preliminary analysis, spectroscopic observations of AS Eri were carried out using the Medium And Low-dispersion Longslit Spectrograph (MALLS) installed on the Nasmyth platform of the 2 m NAYUTA telescope at Nishi-Harima Astronomical Observatory (NHAO). MALLS is equipped with a 2K $\times$ 2K CCD detector (13.5 μm / pixel), by which about 400 Å region can be covered at a spectral resolution of $R \sim 8000$ at 5000 Å in a single exposure (Ozaki and Tokimasa 2005). The journal of the observations is summarized in table 2. Each observation of AS Eri was made at out of eclipses. The orbital phases listed in table 2 were calculated using the ephemeris given in Kreiner (2004).

α PsA (Fomalhaut, A3 V) was chosen as a reference star of AS Eri-p. Since we did not have information about abundances of AS Eri, we assumed that they are the solar aboundances. β Gem (Pollux, K0 III, [Fe/H] = $-0.07\pm$ 0.05; Hatzes et al. 2012) was selected as a reference

star of AS Eri-s. Spectra of α PsA and β Gem were obtained in the same wavelength regions with AS Eri. Reduction of NHAO spectrum was performed using the IRAF[1] software package in a standard manner. The wavelength calibration was performed using an Fe-Ne-Ar lamp.

2.2. Data for Detailed Analysis

High resolution spectral data (R ∼72000) of AS Eri were obtained with the Subaru telescope using High Dispersion Spectrograph (HDS) for a detailed analysis. These observations were carried out under the program ID; S06B-015 (PI; N. Arimoto) as one of the spectroscopic standards from on 2007 January 25 to 29 (UT). The detector of HDS is a mosaic of two 2K × 4K EEV CCD's with 13.5 μm / pixels. Technical details and the performance of the spectrograph are described in Noguchi et al. (2002). Our observations covered two wavelength regions of blue-visual (4400-5700 Å) and visual-red (5800-7000 Å). The journal of the observations is summarized in table 3, in which orbital phases are out of eclipses. We defined the spectra obtained on January 26 (UT) as DATA1 and January 27 (UT) as DATA2, respectively. The exposure time was 60 s in each night. The orbital phases listed in table 3 were calculated using the ephemeris of Kreiner (2004). Th-Ar lamp emission spectra were obtained during the observations at Subaru for the wavelength calibration.

In order to subtract the spectra of AS Eri-s, we observed a K0 III star. As indicated in the next section, a preliminary result showed that the Fe abundance of AS Eri-p is ∼0.8 dex deficient relative to that of the standard star α PsA. Therefore, spectral data of K0 IIIb star ϕ^2 Ori (HD 37160, [Fe/H] = -0.581 ± 0.046; Gray et al. 2002) were obtained on 2007 January 31 (UT) using the HIgh Dispersion Echelle Spectrograph (HIDES, Izumiura 1999) of the 188 cm reflector at Okayama Astrophysical Observatory (OAO). The detector of HIDES is a 4K × 2K CCD. These observations were covered two wavelength regions of blue-visual (4300-5600 Å) and red (6000-7300 Å) with a red cross-disperser. The total exposure time for the target was 3000 s for the blue-visual region, and 1200 s for the red region. A spectral resolution of HIDES was ∼67000 at 5000 Å and ∼70000 at 7000 Å, respectively. The signal-to-noise (SN) ratio (per pixel) of the OAO data was ∼600 at both 4600 Å and 6500 Å. Th-Ar lamp emission spectra were taken at OAO for the wavelength calibration. In order to obtain the missing wavelength region (5600-6000 Å) of HIDES observations, additional HIDES data which cover the wavelength region of ϕ^2 Ori have been downloaded from a website of Subaru-Mitaka-Okayama-Kiso Archive System (SMOKA, Baba et al. 2002). The SN ratio of the data was ∼400 and a spectral resolution was ∼67000 at 5800 Å. For both Subaru and OAO observations, a reduction of two-dimensional spectral data was performed using the IRAF.

High quality spectroscopic data of α PsA have been downloaded from a website of

[1] IRAF is distributed by the National Optical Astronomy Observatories, which are operated by the Association of Universities for Research in Astronomy, Inc., under cooperative agreement with the National Science Foundation.

McDonald Observatory (Allende Prieto 2004). Spectral data of this reference star have a wide wavelength coverage (from 3650 Å to 10400 Å) and a spectral resolution of around 50000. The SN ratio of the data was higher than 500 at 6000 Å . The observational log of α PsA and ϕ^2 Ori is also showed in table 3.

3. Spectroscopic Analysis

3.1. Atmospheric Parameters

Abundances in AS Eri-p were determined using a differential analysis technique relative to the reference star α PsA. The spectral type of this bright spectroscopic standard star is A3 V (Yamashita et al. 1977) which is the same type of AS Eri-p (Mkrtichian et al. 2004). The surface abundances of C, Mg, Si, S, Ca, Ti, Cr, Mn, Fe, and Ni in α PsA are solar within the uncertainties (Dunkin et al. 1997). We assume in this study that α PsA has the normal (solar) abundances of all elements. Atmospheric parameters for α PsA are adopted from Paper I; the effective temperature $T_{\rm eff}$ = 8760 K, the surface gravity log g = 4.2, the microturbulent velocity $\xi_{\rm t}$ = 3.5 $\pm$ 1.0 km s^{-1}, and the rotational velocity v sin i = 89.0 $\pm$ 1.4 km s^{-1}.

The surface gravity log $g_{\rm (p)}$ = 4.33 of AS Eri-p was calculated from the mass of 1.93 $M_{\odot}$and the radius 1.57 $R_{\odot}$which were taken from Mkrtichian et al. (2004). The effective temperature $T_{\rm eff(p)}$ = 8500 K of the AS Eri-p was taken from the same paper.

In order to make a model spectra of AS Eri-s (K0 III), we determined physical parameters as follows. The value of $T_{\rm eff(s)}$ = 4790 K of AS Eri-s was adapted from van Hamme and Wilson (1984). The mass ratio (q = $M_{\rm s}$ / $M_{\rm p}$ =0.1048) was listed in their table 2. From the mass of AS Eri-p, $M_{\rm p}$ = 1.93 $M_{\odot}$(Mkrtichian et al. 2004), we could obtain the mass of AS Eri-s, $M_{\rm s}$ = 0.20 $M_{\odot}$. Together with this value and the radius of AS Eri-s, $R_{\rm s}$ = 2.07 $R_{\odot}$(van Hamme and Wilson 1984), we determined the surface gravity of AS Eri-s to be log $g_{\rm (s)}$ = 3.11. The microturbulent velocity $\xi_{\rm t(s)}$ = 1 km s^{-1} of AS Eri-s was assumed with reference to Takeda et al. (2008). The values of the $T_{\rm eff}$ = 4720 K and log g = 2.30 for ϕ^2 Ori were employed from Allende Prieto et al. (1999) .

3.2. Preliminary Analysis

In order to make a rough estimate, we carried out preliminary analysis. We used data obtained with the NAYUTA/MALLS for this analysis. As a first step, it is necessary to subtract the contribution of AS Eri-s from the observed spectra of AS Eri. The model spectra of AS Eri-s (K0 III) were synthesized by the spectral analysis code (multi-parameter fitting technique) SPTOOL developed by Y. Takeda (Takeda 1995), based on R. L. Kurucz's ATLAS9/WIDTH9 programs (Kurucz 1993). As previously mentioned, the metallicity [M/H] = 0.0 is assumed because we did not know abundances of AS Eri in the first place. We compared the model spectra of AS Eri-s to the observed spectra of β Gem ($T_{\rm eff}$ = 4835 $\pm$ 50 K, log g = 2.70 $\pm$ 0.10, Hatzes et al. 2012), and confirmed that they are almost the same. The line profiles of the

model spectra were broader than the observation because of the synchronous rotation of ∼40 km s^{-1}. The wavelengths of model spectra were shifted corresponding to the orbital phase. Intensity ratios were corrected to match the values of AS Eri-s observed at each observation phase and wavelength. After these calibrations, we subtracted model spectra of AS Eri-s from the observed spectra, and normalized to the continuum of unity. We considered these subtracted data as the spectra of the AS Eri-p.

We found the best value of the microturbulent velocity in AS Eri-p $\xi_{t(p)}$ that satisfy the following two requirements, the independence on the equivalent widths and the ionization balance between Fe I and Fe II. Analyses were carried out by measuring the equivalent widths of unblended lines with the SPTOOL. We used twelve Fe I lines and five Fe II lines to estimate the value, and found the preliminary result of $\xi_{t(p)} \sim 2.7$ km s^{-1}.

α PsA shows broad spectral lines due to its fast rotation (89.0 ± 1.4 km s^{-1}; Paper I). In such a case, reliable measurements of equivalent widths are difficult for broadened absorption lines due to severe blending with neighboring lines. Therefore, we carefully selected the four Fe I lines and one Fe II line which are unblended to be used in the differential abundance analysis. We estimated that the average Fe abundance of the AS Eri-p is ~ -0.8 dex relative to that of α PsA.

3.3. Detailed Analysis

For a detailed analysis, the data of AS Eri obtained with the Subaru/HDS and those of ϕ^2 Ori observed with the OAO/HIDES were used. Since AS Eri is a semi-detached Algol-type system, we assumed that the surface abundances of primary and secondary stars are same. In fact, İbanoğlu et al. (2012) observed such evidence in the many mass-transferring Algol systems. As we described earlier, to determine the surface abundances of primary component, we needed to subtract the contribution of AS Eri-s from the observed spectrum. The observed spectra of ϕ^2 Ori ([Fe/H] = -0.581 ± 0.046) were liken to those of AS Eri-s, because the average Fe abundance of AS Eri-p is estimated to ~ -0.8 dex relative to that of α PsA by the preliminary analysis. The model spectra of K0 III were made by the SPTOOL to validate the spectra of ϕ^2 Ori. The metallicities of [M/H] were fixed to -0.6 in the model spectra. We compared the model spectra to the observed ϕ^2 Ori spectra, and found that both spectra were consistent with each other, except for some special lines (e.g., Ca I auto-ionization level lines, Li I lines). On ϕ^2 Ori, we assumed that the line broadening depends only on the rotational velocity (∼40 km^{-1}), because the effects from other parameters (e.g. instrumental broadening and atmospheric turbulence) to the line broadening are much smaller than that of the rotational velocity.

We corrected the wavelength and the intensity ratio of the AS Eri-s to AS Eri-p in the same manner of preliminary analysis. We then subtracted of ϕ^2 Ori from observed spectra of AS Eri and normalized to the continuum of unity. These subtracted data were considered as

the spectra of the AS Eri-p. Figure 1 shows a comparison between the observed and subtracted spectra ranging from 4951 to 4963 Å of AS Eri based on DATA1.

We estimated the microturbulent velocity of AS Eri-p, $\xi_{t(p)}$ by simulating several spectral features that contain both weak and intermediate strong absorption lines of Fe. Figure 2 is an example of determination of $\xi_{t(p)}$ values. The resulting abundances determined from weak lines are almost independent of the selection of the parameter, while those from relatively strong lines are fairly dependent on the adopted value of $\xi_{t(p)}$. We determined the parameter in order to obtain consistent abundances from both the weak and intermediate strong lines simultaneously. After simulating some spectral regions, we conclude that the best choice is $\xi_{t(p)} = 2.5 \pm 0.3$ km s^{-1}.

We tried to obtain the Fe abundances of AS Eri-p and α PsA with the SPTOOL program using the atmospheric parameters determined in section 3.1. Selected spectral regions are shown in table 4. The major contributing lines are listed for each region. The log *gf* vales were taken from the NIST [2] database. The data given by Kurucz and Bell (1995) were used, when we could not find them in the NIST database. We fixed the microturbulent velocity at the adopted value for each star. The value of -0.8 was adopted as the metallicities of [M/H] based on the preliminary result, and we used three Fe I and four Fe II lines of DATA1 for detailed analysis. However the average abundance of these Fe lines of the AS Eri-p is 0.6 dex lower than that of α PsA. Therefore the metallicities of [M/H] was fixed to -0.6. While the abundance of Fe and the rotational velocity were changed in the fitting calculations.

We used the same wavelength range and the same number of iterations in SPTOOL calculation for AS Eri-p and α PsA. The resulting best-fit values of abundance of Fe for each star are given in table 5. An example of the analysis of Fe region is shown in figure 3. The average abundances of Fe are log N (Fe) $= 7.13 \pm 0.20$, log N (Fe) $= 7.19 \pm 0.18$ and log N (Fe) $= 7.86 \pm 0.15$ for AS Eri-p (DATA1), AS Eri-p (DATA2) and α PsA respectively. We obtained the average Fe abundances of AS Eri-p relative to that of α PsA are -0.68 ± 0.09 dex and -0.64 ± 0.12 dex based on DATA1 and DATA2, respectively. These results show a considerable deficiency of Fe in AS Eri-p.

Next we analyzed the abundances of other metallic elements (Mg, Si, Ca, Ti and Cr) in the same way. A list of the used regions is given in table 6. We changed the abundance of the element and the rotational velocity as adjustable parameters. Some example of the analysis of other elements are showed in figures 4, 5, 6, 7 and 8. The resulting abundances for five elements are summarized in table 7. We conclude that the averaged difference in other elements between AS Eri-p and α PsA are ~ -0.4 dex, which means the metallic deficiency in AS Eri-p. Since the lines of light elements (e.g., C, O and S) are weak and/or blended, we could not analyze them.

The systematic errors in the derived abundances in AS Eri-p caused by uncertainties

[2] http://physics.nist.gov/PhysRefData/ASD/index.html

in the atmospheric parameters are given in table 8. They were estimated by calculating the abundances using model atmospheres with different parameters.

In general, we observe the hot area of the primary star heated by the impact of the gas stream from the secondary star before the mid-primary eclipse in Algol binary systems. Narusawa et al. (2006b) performed spectroscopic observations during two primary eclipse of RZ Cas: they covered 9 and 15 pulsational phases in each night. They reported that changes of equivalent widths (EWs) with the orbital phase are asymmetrical relative to the mid-primary eclipse in RZ Cas (EWs observed before the mid-primary eclipse is smaller than that after mid-primary, see their figure 2). They believed such a phenomenon was due to the existence of a hot spot. We observed AS Eri before and after the mid-primary eclipse, DATA1 (orbital phase = 0.805) and DATA2 (orbital phase = 0.174). The EWs measured from DATA1 and DATA2 of AS Eri-p are given in table 9. We find no systematic differences in the EWs between DATA1 and DATA2. It is known that EWs for NRP stars vary during the pulsational cycle (e.g. Reed et al. 2009, Briquet et al. 2001). Since we observed only 4 percent of the pulsational phase of AS Eri-p in each night, it is not clear how much the NRP influenced EWs at that time. Therefore it is difficult to obtain information about existence of a hot spot. None the less, our abundance analyses based on DATA1 and DATA2 agree within the margin of the error bar ($\sim \pm 0.1$). Hence we conclude that the NRP and a hot spot (if it exist) do not have any significant influences on the chemical abundances in AS Eri-p.

3.4. Rotational Velocity

Observed rotational velocities in many mass-transfer systems are faster than synchronous rotation velocities due to the accelerating effect of angular momentum accretion process (Packet 1981). If mass-transfer mechanism does not work in AS Eri, the synchronous rotation of AS Eri-p is expected to be $V_{\rm syn(p)} = 30$ km s^{-1}. [3] The rotational velocity of AS Eri-p was computed with selected 43 absorption lines from six elements using the multiple parameter fitting program (MPFIT, part of the SPTOOL). We obtained the rotational velocity (v sin i) of 39.9 $\pm$ 2.8 km s $^{-1}$, indicating that AS Eri belongs to the mass-transfer system. This result is somewhat different from previous studies, e.g. $V_{\rm rot(p)}$ $\sim$35 km s^{-1} (Popper 1973) and 46 km s^{-1} (Levato 1974). Olson (1984) suggested that some Algol-type systems showed changes of the rotational velocity due to the sporadic flows.

4. Discussion

We have carried out abundances analysis of AS Eri-p, and found definite under-abundances of six elements: Mg, Si, Ca, Ti, Cr and Fe. Our final results are presented in table 10. For a comparison, data of RZ Cas-p are listed in the table. RZ Cas-p shows a charac-

[3] $V_{\rm syn(p)} = 2\ \pi\ R_{\rm p}\ /\ P_{\rm rot}$, where $P_{\rm rot}$ is rotational period. The values of $R_{\rm p} = 1.57\ R_{\odot} (= 1.09 * 10^6$ km) and $P_{\rm rot}$ $(= P_{\rm orb}) = 2.6642$ day $(= 2.3019 * 10^5$ sec) in the present case.

teristic of mild λ Boötis-type stars (Paper I). Unfortunately, we could not analyze light element of AS Eri-p, it is unclear wheather this is a λ Boötis-type star or not. Anyway, we regard that both stars are not Ap star. It is difficult to adopt the diffusion (radiative levitation and gravity setting) model to the primary components of Algol systems whose atmosphere is dynamic (due to the direct impact of mass from a secondary star).

We discuss the similarity of three pulsating stars; AS Eri-p, RZ Cas-p and V1366 Ori (HD 34282). V1366 Ori is an A3 V δ Sct (and Herbig Ae) star and its period of 18.13 min (Casey et al. 2013) is almost the same as periods of both AS Eri-p and RZ Cas-p. Merín et al. (2004) reported that abundance of Fe ([Fe/H]) in V1366 Ori is -0.8 ± 0.1 (this star dose not seem to be a λ Boö-type, Amado et al. 2006). Physical parameters and pulsational features of AS Eri-p, RZ Cas-p and V1366 Ori are summarized in table 11 and table 12, respectively. We conclude that AS Eri-p, RZ Cas-p and V1366 Ori have much similar pulsational period ($P_{\rm puls}$ $\sim$ 20 min) and under abundance of metallic elements. Here, we call these three short period pulsators the "ASE-type", for convenience.

To compare the ASE-type and the solar abundant pulsator, we refer to a component of eclipsing system RS Chamaeleontis. This star is the δ Sct type whose surface metallicities are determined. The Fe abundance ([Fe/H]) of this star is $+0.17 \pm 0.01$ (Alecian et al. 2005) and the pulsational period is $P_{\rm puls} = 2.06$ hr, which is much longer than that of ASE-type. Therefore, there may be a correlation between pulsational periods and metallicities in ASE-type.

On the other hand, these are pulsating λ Boötis-type stars (e.g., 35 Aql, λ Boo and 29 Cyg). The Fe abundance [Fe/H] of 35 Aql, λ Boo and 29 Cyg are -1.6, -2.0 and -2.0, respectively (Venn and Lambert 1990, Heiter et al. 1998). If short periods are driven solely by metal deficiency, the periods of these stars should be shorter than ASE-type. However the periods of 35 Aql, λ Boo and 29 Cyg are 30 min, 33 min and 41 min for, respectively (Paunzen et al. 2002).

We speculate that the mass-transfer/accretion and/or magnetic field cause an atmospheric structure which has predisposition toward oscillatory instability. Retter at al. (2005) suggested that Algol-type is reminiscent of magnetic active binary star RS CVn systems. They proposed that magnetized accretion annulus exist around the early type primary components. On the other hand, a large Keplerian disk around Herbig Ae star V1366 Ori was found by Piétu et al. (2003). Mel'nikov (2004) suggested that large amount of circumstellar matters fall onto the Herbig Ae/Be stars. Moreover, Hubrig et al. (2011) reported that magnetic fields were detected in Herbig Ae/Be stars.

We guess that not only metal deficiency but also the mass-transfer/accretion and/or magnetic field are related with pulsational periods. However, it is necessary to conduct spectral analysis of many oscillational components of binary systems to clarify the physical relation among the pulsational characteristics, metal abundances, and atmospheric structures.

We thank H. Naito, S. Ozaki and staff members of Okayama Astrophysical Observatory and Nishi-Harima Astronomical Observatory for their help during our observations. We express their sincere thanks to N. Arimoto, W. Aoki, A. Tajitsu, S. Kawanomoto for providing the Subaru/HDS data of AS Eri. Thanks are also due to Y. Takeda for providing us with his spectral analysis code SPTOOL. We are grateful to K. Tanaka, E. Kambe, K. Sadakane and M. Takada-Hidai for useful comments.

References

Alecian, E., Catala, C., Van't Veer-Menneret, C., Goupil, M.-J., & Balona, L. 2005, A&A, 442, 993

Alentiev, D., Kochukhov, O., Ryabchikova, T., Cunha, M., Tsymbal, V., & Weiss, W. 2012, MNRAS, 421, L82

Allende Prieto, C., García López, R., Lambert, D.L., & Gustafsson, B. 1999, ApJ, 527, 879

Allende Prieto, C., Barklem, P. S., Lambert, D.L., & Cunha, K. 2004, A&A, 420, 183 (spectral data were retrieved from: http://hebe.as.utexas.edu/s4n/)

Amado, P. J., Rodríguez, E., Choo, Kyung-J., Kim, S. -L., Garrido, R., Suárez, J. C., Moya, A., & Martín-Ruiz, S. 2006, Mem. Soc. Astron. Italiana, 77, 97

Baba, H., et al. 2002, in ASP Conf. Ser., 281, Astronomical Data Analysis Software and Systems XI, ed. D. A. Bohlender, D. Durand & T. H. Handley (San Francisco: ASP), 298

Balona, L. A., et al. 2012, MNRAS, 424, 1187

Breger, M. 2000, in ASP Conf. Ser., 210, Delta Scuti and Related Stars, Reference Handbook and Proceedings of the 60th Vienna Workshop in Astrophysics, ed. M. Breger & M. H. Montgomery (San Francisco: ASP), 3

Briquet, M., De Cat, P., Aerts, C. & Scuflaire, R. 2001, A&A, 380, 177

Casey, M. P., et al. 2013, MNRAS, 428, 2596

Damiani, C., Maceroni, C., Cardini, D., Debosscher, J., Balaguer-Núñez, L., & Ribas, I. 2010, Ap&SS, 328, 91

Derekas, A., et al. 2009, MNRAS, 394, 995

Dimitrov, D., Kraicheva, Z., Popov, V., & Genkov, V. 2010, Inf. Bull. Var. Stars, 5925

Dunkin, S. K., Barlow, M. J., & Ryan, S. G. 1997, MNRAS, 286, 604

Gamarova, A.Yu., Mkrtichian, D. E., & Kusakin, A. V. 2000, Inf. Bull. Var. Stars, 4837

Gray, D. F., Scott, H. R., & Postma, J. E. 2002, PASP, 114, 536

Hambsch, F-J., Lampens, P., van Cauteren, P., Kleidis, S., Robertson, C. W., Krajci, T., & Wils, P. 2010 Inf. Bull. Var. Stars, 5949

Hatzes, A. P., et al. 2012, A&A, 543, A98

Heiter, U., Kupka, F., Paunzen, E., Weiss, W. W., & Gelbmann, M. 1998. A&A, 335, 1009

Hoffmeister, C. 1934, Astron. Nachr., 253, 195

Hubrig, S., et al. 2011, Astron. Nachr., 332, 1022

İbanoğlu, C., Dervişoğlu, A., Çakırlı, Ö., Sipahi, E., & Yüce, K. 2012, MNRAS, 419, 1472

Izumiura, H. 1999, in Proc. 4th East Asian Meeting on Astronomy, ed. P. S. Chen (Kunming, Yunnan Observatory), 77

Kreiner, J. M. 2004, Acta Astron., 54, 207
Kurtz, D. W. 1990, ARA&A, 28, 607
Kurucz, R. 1993, Kurucz CD-ROM, No.13 (Harvard-Smithsonian Center for Astrophysics)
Kurucz, R., & Bell, B. 1995, Kurucz CD-ROM, No.23 (Harvard-Smithsonian Center for Astrophysics)
Lehmann, H., & Mkrtichian, D. E. 2008, A&A, 480, 247
Levato, H. 1974, A&A, 35, 259
Liakos, A., Niarchos, P., Soydugan, E., & Zasche, P. 2012 MNRAS, 422, 1250
Mel'nikov, S. Yu. 2004, Baltic Astron., 13, 548
Merín, B., et al. 2004, A&A, 419, 301
Mkrtichian, D. E., Kusakin, A. V., Gamarova, A.Yu., & Nazarenko, V. 2002, in ASP Conf. Ser., 259, Radial and Nonradial Pulsations as Probes of Stellar Physics, ed. C. Aerts, T.R. Bedding & J. Christensen-Dalsgaard (San Francisco: ASP), 96
Mkrtichian, D. E., et al. 2003, in ASP Conf. Ser., 292, Interplay of Periodic, Cyclic and Stochastic Variability in Selected Areas of the H-R Diagram, ed. C. Sterken (San Francisco: ASP), 113
Mkrtichian, D. E., et al. 2004, A&A, 419, 1015
Mkrtichian, D. E., Rodríguez, E., Olson, E. C., Kusakin, A. V., Kim, S.-L., Lehmann, H., Gamarova, A.Yu., & Kang, Y. W. 2005, in ASP Conf. Ser., 333, Tidal Evolution and Oscillations in Binary Stars: Third Granada Workshop on Stellar Structure, ed. A. Claret, A. Giménez & J. -P. Zahn (San Francisco: ASP), 197
Mkrtichian, D. E., et al. 2007, in ASP Conf. Ser. 370, Solar and Stellar Physics Through Eclipses, ed. O. Demircan, S. O. Selam & B. Albayrak (San Francisco: ASP), 194
Narusawa, S., Ozaki, S., Kambe, E., & Sadakane, K. 2006a, PASJ, 58, 617 (Paper I)
Narusawa, S., Ozaki, S., Okyudo, M., Takano, R., & Nakamura, Y. 2006b, PASP, 118, 809
Noguchi, K., et al. 2002, PASJ, 54, 855
Norris, J. E., Ryan, S. G. & Beers, T. C. 2001, ApJ, 561, 1034
Ohshima, O., Narusawa, S., Akazawa, H., Fujii, M., Kawabata, T., & Ohkura, N. 1998, Inf. Bull. Var. Stars, 4581
Ohshima, O., et al. 2001, AJ, 122, 418
Olson, E. C. 1984, PASP, 96, 376
Ozaki, S., & Tokimasa, N. 2005, Ann. Rep. Nishi-Harima Astron. Obs., 15, 15 (in Japanese)
Packet, W. 1981, A&A, 102, 17
Paunzen, E., et al. 2002 A&A, 392, 515
Paunzen, E. 2004, in Proc. IAU Symp. 224, The A-Star Puzzle, ed. J. Zverko, J. Žižňovský, S. J. Adelman & W. W. Weiss (Cambridge: Cambridge Univ. Press), 443
Piétu, V., Dutrey, A., & Kahane, C. 2003, A&A, 398, 565
Popper, D. M. 1973, ApJ, 185, 265
Reed, M. D., et al. 2009, A&A, 493, 175
Retter, A., Richards, M.T., & Wu, K. 2005, ApJ, 621, 417
Rodríguez, E., et al. 2004, MNRAS, 347, 1317
Southworth, J., et al. 2011, MNRAS, 414, 2413
Soydugan, E., Soydugan, F., Demircan, O., & İbanoğlu, C. 2006, MNRAS, 370, 2013

Takeda, Y. 1995, PASJ, 47, 287
Takeda, Y., Sato, B., & Murata, D. 2008, PASJ, 60, 781
Tempesti, P. 1971, Inf. Bull. Var. Stars, 596
Uytterhoeven, K., et al. 2011, A&A, 534, A125
van Hamme, W., & Wilson, R. E. 1984, A&A, 141, 1
Venn, K. A., & Lambert, D. L. 1990, ApJ, 363, 234
Yamashita, Y., Nariai, K., & Norimoto, Y. 1977, An Atlas of Representative Stellar Spectra (Tokyo: University of Tokyo Press)
Zhou A. -Y. 2010, preprint (arXiv:1002.2729v4)

Table 1. Data of stars

Star	HD number	m_v [a]	Sp. Type	Comments
AS Eri	21985	8.30	A3 V+K0 III	EA/SD, target star
α PsA (Fomalhaut)	216956	1.16	A3 V	Reference star for AS Eri-p
β Gem (Pollux)	62509	1.15	K0 III	Reference star for AS Eri-s (Preliminary Analysis)
ϕ^2 Ori	37160	4.09	K0 III b	Reference star for AS Eri-s (Detailed Analysis)

a: SIMBAD Astronomical Database (http://simbad.u-strasbg.fr/simbad/)

Table 2. Observational Log of AS Eri, α PsA and β Gem with the NAYUTA.

Star	Date (UT)	central wavelength (Å)	total exposure time (s)	S/N	orbital phase (at the central time)
AS Eri	Dec. 15 2005	4341	7800	∼400	0.189
	Jan. 23 2006	5200	6000	∼700	0.789
	Jan. 28 2006	5895	8880	∼600	0.687
	Feb. 1 2006	5450	9000	∼600	0.179
	Feb. 9 2006	4861	5400	∼500	0.179
	Feb. 13 2006	6156	10800	∼700	0.674
	Oct. 8 2006	6563	9000	∼600	0.731
α PsA	Nov. 15 2005	4861	60	∼800	-
	Aug. 3 2006	5200	200	∼1100	-
		5450	200	∼1100	-
		5895	100	∼700	-
	Aug. 6 2006	4341	150	∼600	-
		6156	40	∼500	-
	Aug. 15 2006	6563	25	∼700	-
	Aug. 25 2006	3968	145	∼100	-
	Dec. 19 2006	4650	90	∼1200	-
β Gem	Apr. 25 2006	4341	65	∼600	-
		4861	19	∼700	-
		5200	13	∼700	-
		5450	13	∼700	-
		5890	13	∼700	-
		6563	16	∼700	-
	Dec. 19 2007	6250	21	∼700	-
	Mar. 25 2007	4650	90	∼1400	-

Table 3. Observational log of AS Eri with the Subaru and related stars.

	AS Eri (DATA1)	AS Eri (DATA2)	α PsA	ϕ^2 Ori	ϕ^2 Ori
observatory	Subaru	Subaru	McDonald	OAO	OAO
			(Allende Prieto 2004)		(SMOKA)
date (UT)	Jan. 26 2007	Jan. 27 2007		Jan. 31 2007	Jan. 23 2004
wavelength region (Å)	4400-5700	4400-5700	3650-10400	4300-5600	5600-6000
	5800-7000	5800-7000		6000-7300	
exp. time (s)	60	60		3000 (4300-5600 Å)	600
				1200 (6000-7300 Å)	
resolution	72000	72000	50000	67000 (5000 Å)	67000 (5800 Å)
				70000 (7000 Å)	
S/N	∼300	∼200	∼500 (at 6000 Å)	∼600	∼400
orbital phase	0.805	0.174	-	-	-

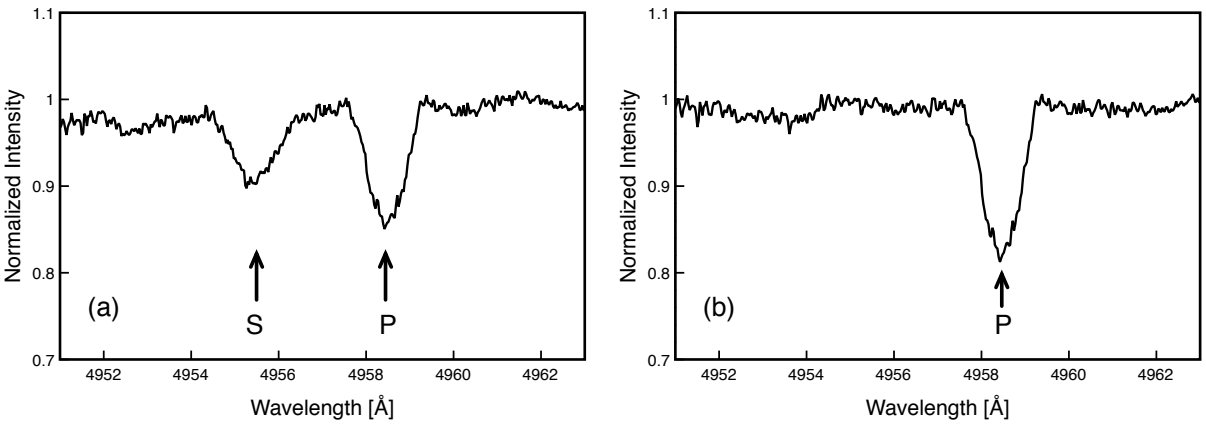

Fig. 1. A comparison between the observed (a) and subtracted (b) spectra of AS Eri (DATA1). P and S show absorption lines of primary and secondary component, respectively. The absorption line of the secondary is not shown in the subtracted spectra.

Table 4. Used wavelength regions of Fe lines.

Region	λ 1 (Å)	λ 2 (Å)	Lines	χ (eV)	log gf	Reference[a]
A	4403.0	4407.0	Fe I 4404.750	1.557	−0.142	1
B	4474.0	4479.0	Fe I 4476.017	2.845	−0.570	2
			Fe I 4476.077	3.686	−0.370	2
C	4505.0	4512.0	Fe II 4508.288	2.856	−2.21	1
D	4512.0	4518.0	Fe II 4515.339	2.844	−2.48	1
E	4518.0	4525.0	Fe II 4520.224	2.807	−2.61	1
			Fe II 4522.634	2.844	−2.03	1
F	4574.0	4578.5	Fe II 4576.340	2.844	−3.04	1
G	4627.3	4632.0	Fe II 4629.339	2.807	−2.38	1
H	4675.0	4684.0	Fe I 4678.845	3.603	−0.66	1
I	4728.5	4734.0	Fe II 4731.453	2.891	−3.37	1
J	4734.0	4739.5	Fe I 4735.842	4.076	−1.23	1
			Fe I 4736.772	3.211	−0.74	1
K	5015.0	5023.0	Fe II 5018.440	2.891	−1.21	1
L	5360.0	5375.0	Fe II 5362.869	3.199	−2.739	2
			Fe I 5364.858	4.446	0.22	1
			Fe I 5367.479	4.415	0.35	1
			Fe I 5369.958	4.371	0.35	1
			Fe I 5371.489	0.958	−1.644	1
			Fe I 5371.596	4.312	−0.780	2
			Fe I 5373.698	4.473	−0.87	1
M	5421.5	5427.5	Fe I 5424.069	4.320	0.52	1
			Fe II 5425.257	3.199	−3.36	1
N	5440.0	5453.0	Fe I 5445.042	4.386	−0.01	1
			Fe I 5446.916	0.990	−1.93	1
O	5452.0	5460.0	Fe I 5455.441	4.320	0.291	2
			Fe I 5455.609	1.011	−1.754	2
P	5532.0	5538.0	Fe II 5534.847	3.245	−2.92	1
			Fe I 5535.417	4.186	−0.749	2
Q	5567.5	5575.5	Fe I 5569.618	3.417	−0.53	1
			Fe I 5572.841	3.397	−0.31	1
R	5610.0	5620.0	Fe I 5615.644	3.332	−0.14	1
S	6062.5	6070.0	Fe I 6065.482	2.609	−1.53	1
T	6075.0	6082.0	Fe I 6078.491	4.795	−0.424	2
			Fe I 6078.999	4.652	−1.13	1
U	6081.0	6087.0	Fe II 6084.111	3.199	−3.97	1
V	6134.0	6140.0	Fe I 6136.615	2.453	−1.399	1
			Fe I 6137.694	2.588	−1.403	1
W	6145.0	6153.0	Fe II 6147.741	3.889	−2.721	2
			Fe II 6149.258	3.889	−2.90	1
X	6185.0	6198.0	Fe I 6191.558	2.433	−1.60	1
Y	6410.0	6424.0	Fe I 6411.647	3.654	−0.82	1
			Fe II 6416.919	3.892	−2.85	1
			Fe I 6419.942	4.733	−0.25	1
			Fe I 6421.349	2.279	−2.027	1

a: 1.Taken from the NIST database. 2. Taken from Kurucz and Bell (1995)

Table 5. Analysis of Fe lines.

Region	λ 1	λ 2	log N (Fe) AS Eri-p (DATA1)	log N (Fe) AS Eri-p (DATA2)	log N (Fe) α PsA	Difference AS Eri-p (DATA1)	Difference AS Eri-p (DATA2)
	(Å)	(Å)	(dex)	(dex)	(dex)	(dex)	(dex)
A	4403.0	4407.0	7.03	7.28	7.73	−0.70	−0.45
B	4474.0	4479.0	6.82		7.44	−0.62	
C	4505.0	4512.0	7.18	7.31	7.81	−0.63	−0.50
D	4512.0	4518.0		7.38	7.89		−0.51
E	4518.0	4525.0	7.14	7.21	7.99	−0.85	−0.78
F	4574.0	4578.5		7.23	7.86		−0.63
G	4627.3	4632.0	7.14	7.17	7.87	−0.73	−0.70
H	4675.0	4684.0			8.00		
I	4728.5	4734.0	7.48	7.47	8.10	−0.62	−0.63
J	4734.0	4739.5			8.01		
K	5015.0	5023.0	7.36	7.10	7.89	−0.53	−0.79
L	5360.0	5375.0			7.87		
M	5421.5	5427.5			7.87		
N	5440.0	5453.0	7.16		7.89	−0.73	
O	5452.0	5460.0	6.86	6.83	7.59	−0.73	−0.76
P	5532.0	5538.0		7.35	7.90		−0.55
Q	5567.5	5575.5		7.00	7.63		−0.63
R	5610.0	5620.0		6.93	7.71		−0.78
S	6062.5	6070.0			7.74		
T	6075.0	6082.0			8.03		
U	6081.0	6087.0			8.02		
V	6134.0	6140.0			7.78		
W	6145.0	6153.0			8.00		
X	6185.0	6198.0			7.88		
Y	6410.0	6424.0			7.88		
averages			7.13 ± 0.20	7.19 ± 0.18	7.86 ±0.15	−0.68 ±0.09	−0.64 ±0.12

Table 6. Used wavelength regions of other elements.

Element	λ 1 (Å)	λ 2 (Å)	Lines	χ (eV)	log gf [a]
Mg I	4701.0	4705.5	Mg I 4702.991	4.346	−0.440
	5163.0	5178.0	Mg I 5167.321	2.709	−0.870
			Mg I 5172.684	2.712	−0.393
Si II	5053.0	5059.0	Si II 5055.984	10.074	0.523
			Si II 5056.317	10.074	−0.492
	6340.0	6355.0	Si II 6347.109	8.121	0.149
	6365.0	6380.0	Si II 6371.371	8.121	−0.082
Ca I	5580.0	5585.0	Ca I 5581.965	2.523	−0.71
	5585.0	5592.5	Ca I 5588.749	2.526	0.21
			Ca I 5590.114	2.521	−0.71
	5855.0	5860.0	Ca I 5857.451	2.933	0.23
	6117.5	6126.0	Ca I 6122.217	1.886	−0.315
	6160.0	6166.0	Ca I 6162.173	1.899	−0.089
	6435.0	6444.0	Ca I 6439.075	2.526	0.47
Ti II	4466.0	4472.0	Ti II 4468.507	1.131	−0.62
	4498.0	4505.0	Ti II 4501.273	1.116	−0.75
	4530.0	4540.0	Ti II 4533.969	1.237	−0.77
	4568.0	4575.0	Ti II 4571.968	1.572	−0.52
	4802.0	4809.0	Ti II 4805.085	2.061	−1.12
Cr II	4632.0	4637.0	Cr II 4634.070	4.072	−1.24
	5310.0	5315.0	Cr II 5313.563	4.073	−1.65

a: Taken from the NIST database.

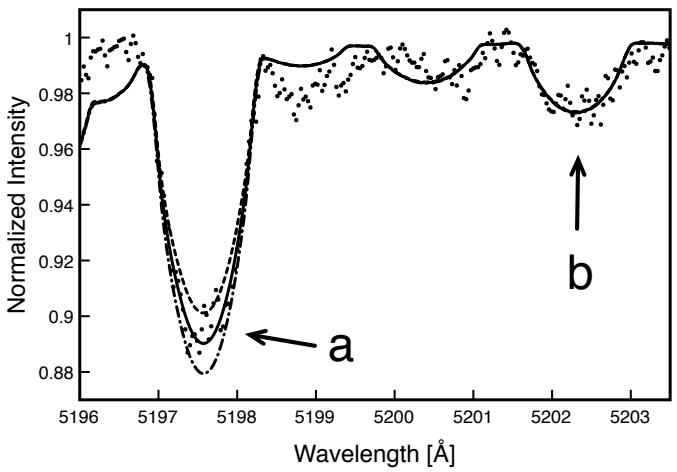

Fig. 2. Microturbulent velocity, $\xi_{t(p)}$ of AS Eri-p. A small section of the observed spectrum between 5196.5 and 5203.5 Åis shown by dots. Simulated spectra, calculated assuming the log N (Fe) = 7.2, for $\xi_{t(p)}$=2.0, 2.5, and 3.0 km s^{-1} are represented by broken, thick solid and chain lines, respectively. Regions a and b contain intermediately strong and weak Fe lines, respectively, and both features can be reproduced when we use $\xi_{t(p)}$=2.5 km s^{-1}.

Table 7. Analysis of other elements.

Element	λ 1	λ 2	log N (X) AS Eri-p (DATA1)	log N (X) AS Eri-p (DATA2)	log N (X) α PsA	Difference AS Eri-p (DATA1)	Difference AS Eri-p (DATA2)
	(Å)	(Å)	(dex)	(dex)	(dex)	(dex)	(dex)
Mg I	4701.0	4705.5	6.91	7.11	7.48	−0.57	−0.37
	5163.0	5178.0	7.07	7.28	7.84	−0.77	−0.56
Si II	5053.0	5059.0		7.64	7.71		−0.07
	6340.0	6355.0	7.95	7.84	7.99	−0.04	−0.15
	6365.0	6380.0			7.88		
Ca I	5580.0	5585.0			6.63		
	5585.0	5592.5	5.71	5.78	6.42	−0.71	−0.64
	5855.0	5860.0	5.83	5.96	6.46	−0.63	−0.50
	6117.5	6126.0	5.81	5.88	6.45	−0.64	−0.57
	6160.0	6166.0	5.86	5.76	6.36	−0.50	−0.60
	6435.0	6444.0			6.41		
Ti II	4466.0	4472.0	4.54		4.76	−0.22	
	4498.0	4505.0	4.71	4.87	5.37	−0.66	−0.50
	4530.0	4540.0			5.32		
	4568.0	4575.0		5.12	5.64		−0.52
	4802.0	4809.0			5.23		
Cr II	4632.0	4637.0		5.74	6.20		−0.46
	5310.0	5315.0	5.77	5.65	5.94	−0.17	−0.29

Table 8. The systematic error analyses.

Element	Δ $T_{\rm eff}$ +200 K	Δ log g −0.3 dex	Δ $\xi_{\rm t}$ -0.3 km s^{-1}	Δ [M/H] −0.3 dex	Total Error[a] (dex)
Mg I	+0.12	+0.05	+0.07	−0.07	0.16
Si II	−0.03	−0.03	+0.07	+0.03	0.09
Ca I	+0.13	+0.04	+0.02	−0.11	0.18
Ti II	+0.09	−0.05	+0.12	−0.02	0.16
Cr II	+0.03	−0.05	+0.03	−0.06	0.09
Fe I	+0.17	+0.03	+0.06	−0.02	0.18
Fe II	+0.08	−0.05	+0.09	−0.01	0.13

a: The total error is obtained by adding four uncertainties in quadrature.

Table 9. Equivalent widths of AS Eri-p.

Element	λ	χ	log gf [a]	$W_\lambda(\sigma)^b$ (DATA1)	W_λ $(\sigma)^b$ (DATA2)	ΔW_λ (DATA1-DATA2)
	(Å)	(eV)		(mÅ)	(mÅ)	(mÅ)
Fe I	4404.750	1.557	−0.142	145(1)	167(2)	−22
Fe I	4476.017	2.845	−0.570	64(1)		
Fe I	4476.077[c]	3.686	−0.370			
Fe II	4508.288	2.856	−2.21	133(2)	138(2)	−5
Fe II	4515.339	2.844	−2.48		128(2)	
Fe II	4520.224	2.807	−2.61	105(2)	101(2)	4
Fe II	4522.634	2.844	−2.03	137(2)	156(2)	−19
Fe II	4576.340	2.844	−3.04		76(2)	
Fe II	4629.339	2.807	−2.38	125(2)	119(2)	6
Fe II	4731.453	2.891	−3.37	62(2)	77(2)	−15
Fe II	5018.440	2.891	−1.21	234(2)	202(3)	32
Fe I	5445.042	4.386	−0.01	56(2)		
Fe I	5446.916	0.990	−1.93	85(2)		
Fe I	5455.441	4.320	0.291	101(2)	96(3)	5
Fe I	5455.609[c]	1.011	−1.754			
Fe II	5534.847	3.245	−2.92		88(3)	
Fe I	5535.417[c]	4.186	−0.749			
Fe I	5569.618	3.417	−0.53		33(3)	
Fe I	5572.841	3.397	−0.31		63(3)	
Fe I	5615.644	3.332	−0.14		80(3)	
Mg I	4702.991	4.346	−0.440	107(2)	135(2)	−28
Mg I	5167.321	2.709	−0.870	236(2)	220(3)	16
Mg I	5172.684	2.712	−0.393	199(2)	254(3)	−55
Si II	5055.984	10.074	0.523		136(3)	
Si II	6347.109	8.121	0.149	228(2)	215(4)	13
Ca I	5588.749	2.526	0.21	48(2)	56(3)	−8
Ca I	5857.451	2.933	0.23	57(2)	51(3)	6
Ca I	6122.217	1.886	−0.315	54(2)	71(3)	−17
Ca I	6162.173	1.899	−0.089	67(2)	62(3)	5
Ti II	4468.507	1.131	−0.62	174(2)		
Ti II	4501.273	1.116	−0.75	136(2)	150(2)	−14
Ti II	4571.968	1.572	−0.52		169(2)	
Cr II	4634.070	4.072	−1.24		78(2)	
Cr II	5313.563	4.073	−1.65	60(2)	52(3)	8

a: The reference is the same as table 4 and 6.

b: Errors (σ) of EWs were obtained by an equation in Norris et al (2001).

c: blended in above line

Table 10. Summary of aboundances in the AS Eri-p and RZ Cas-p.

Element	AS Eri-p[a]	RZ Cas-p[b]
Mg I	−0.57±0.14	−0.36
Mg II		−0.55
Si II	−0.09±0.05	−0.59
Ca I	−0.60±0.07	−0.32
Ti II	−0.48±0.16	−0.45
Cr I		−0.95
Cr II	−0.31±0.12	−0.84
Fe I, Fe II	−0.66±0.11	−0.63

a: this study(average of DATA1 and DATA2), b: Papre I

Table 11. Physical parameters of primary components of RZ Cas, AS Eri and V1366 Ori.

Star	Sp. Type	$M/M_\odot$	$R/R_\odot$	$\log T_{\rm eff}$	$\log L/L_\odot$	$V_{\rm rot}$ (km s^{-1})	abundance (dex)
AS Eri-p	A3 V	1.93	1.57	3.928	1.06	40 [a]	−0.65 [a]
RZ Cas-p	A3 V	2.205	1.67	3.934	1.12	71 [b]	−0.63 [b]
V1366 Ori	A3 V	1.59		3.936	1.13	110	−0.8 ±0.1

a: this study b: Papre I, other parameters of AS Eri-p and RZ Cas-p are taken from Mkrtichian et al. (2004), and parameters of V1366 Ori are taken from Merín et al. (2004)

Table 12. Pulsational features of primary components of RZ Cas-p, AS Eri-p and V1366 Ori

Star	$P_{\rm puls}$ (dominant) (min)	Q (dominant) (day)	mode
AS Eri-p	24.39	0.0120	(l, m, n)=(1, 1, 5) or (2, 2, 5) and (l, m, n)=(2, −2, 6)
RZ Cas-p	22.41[a]	0.011[b]	$l = 2$, $\|m\| = 1, 2$, $n = 6$ [b]
V1366 Ori	18.13		$l = 0, 2$, $n = 13 - 20$

a: Lehmann and Mkrtichian (2008), b: Rodríguez et al. (2004), Parameters of AS Eri-p and V1366 Ori are taken form Mkrtichian et al. (2004) and Casey et al. (2013), respectively

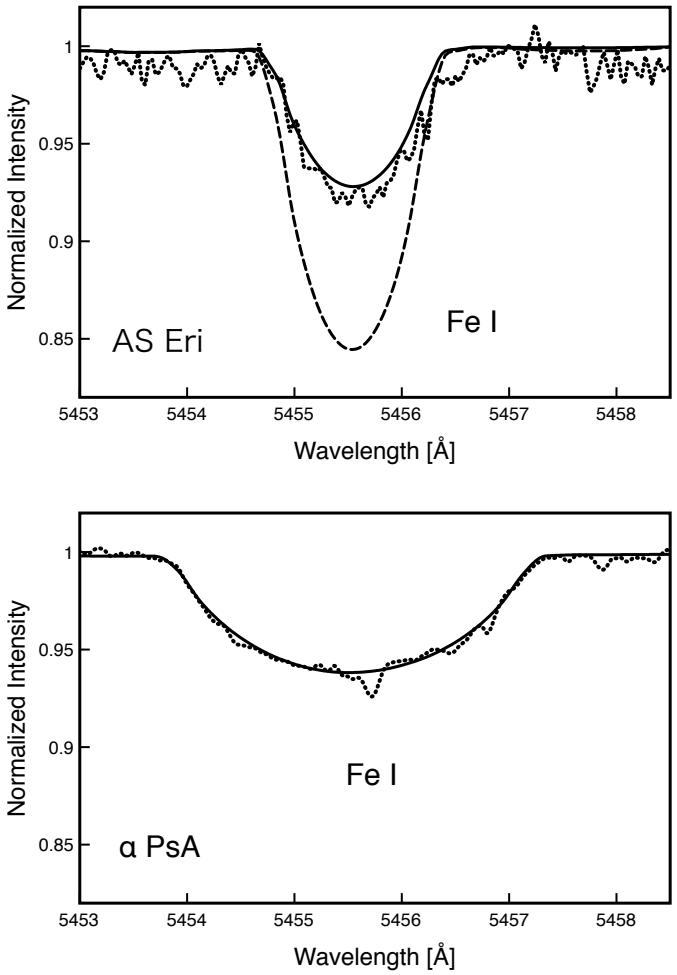

Fig. 3. Spectral synthesis analysis of Fe I feature near 5455 Å. Observed spectra and final fit solutions are shown by dots and solid lines, respectively. Resulting abundances of Fe obtained from this spectral segment are log N(Fe) = 6.86 and 7.59 in AS Eri-p (DATA1) and α PsA, respectively. The dashed line for AS Eri-p represents a simulation for the case of log N(Fe) = 7.59.

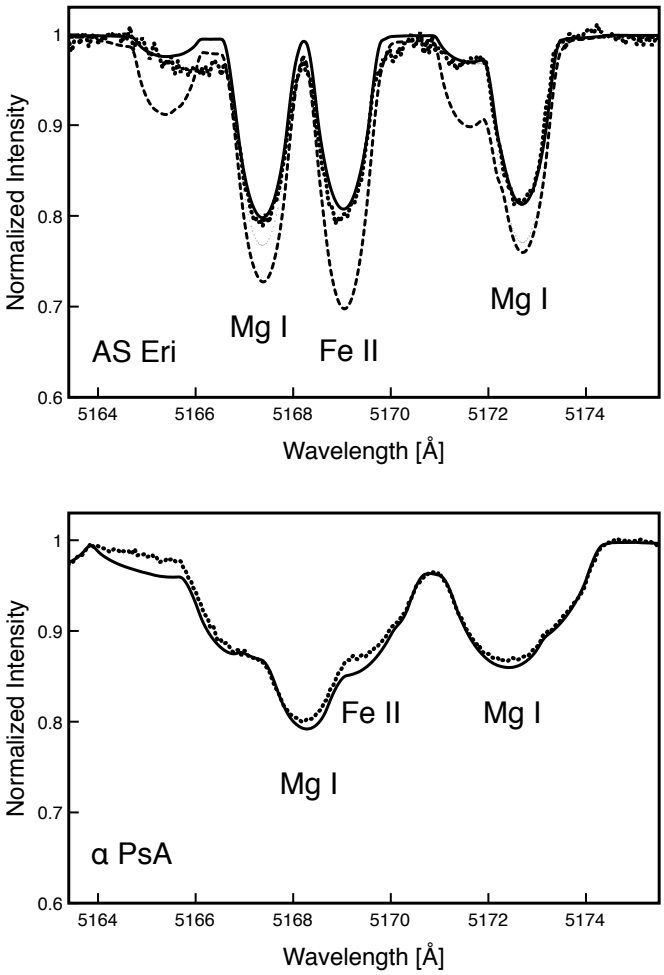

Fig. 4. Spectral synthesis analysis of Mg I feature near 5167 Å. Obseved spectra and final fit solutions are shown by dots and solid lines, respectively. Resulting abundances of Mg obtained from this spectral segment are log $N(\mathrm{Mg}) = 7.07$ and 7.84 in AS Eri (DATA1) and α PsA, respectively. The dashed line for AS Eri represents a simulation for the case of log $N(\mathrm{Mg}) = 7.84$.

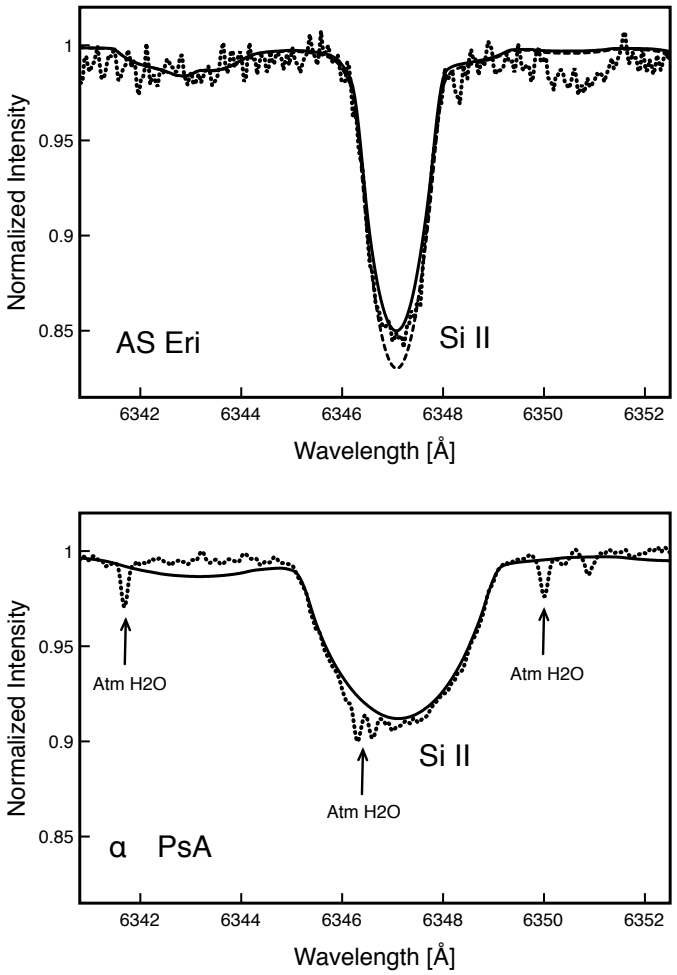

Fig. 5. Spectral synthesis analysis of Si II feature near 6347 Å. Obseved spectra and final fit solutions are shown by dots and solid lines, respectively. Resulting abundances of Si obtained from this spectral segment are log N(Si) = 7.84 and 7.99 in AS Eri-p (DATA2) and α PsA, respectively. The dashed line for AS Eri-p represents a simulation for the case of log N(Si) = 7.99

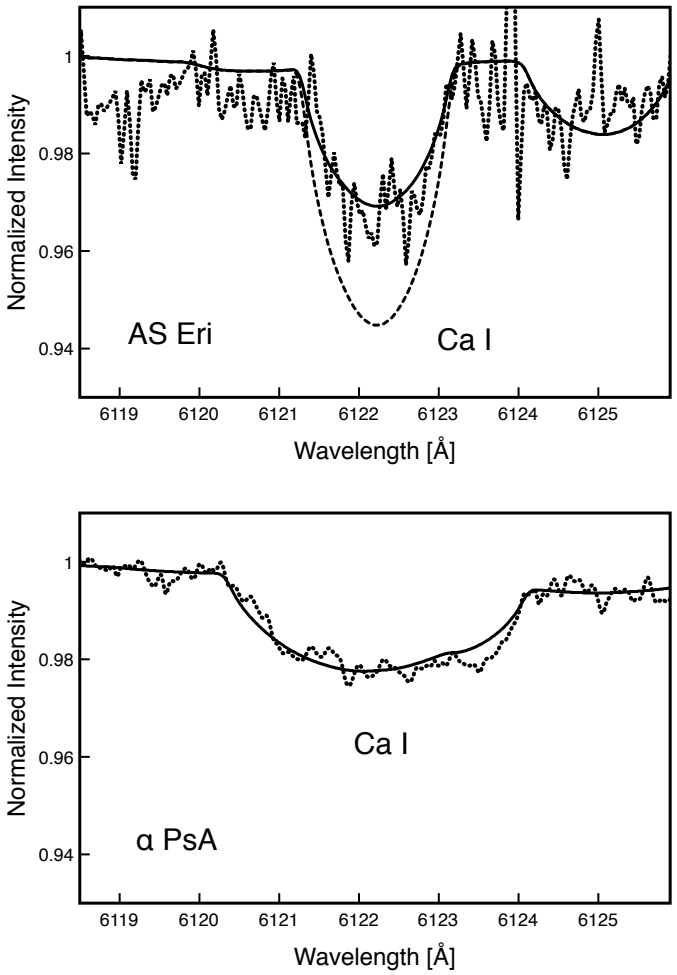

Fig. 6. Spectral synthesis analysis of Ca I feature near 6122 Å. Obseved spectra and final fit solutions are shown by dots and solid lines, respectively. Resulting abundances of Ca obtained from this spectral segment are log N(Ca) = 5.81 and 6.45 in AS Eri-p (DATA1) and α PsA, respectively. The dashed line for AS Eri-p represents a simulation for the case of log N(Ca) = 6.45.

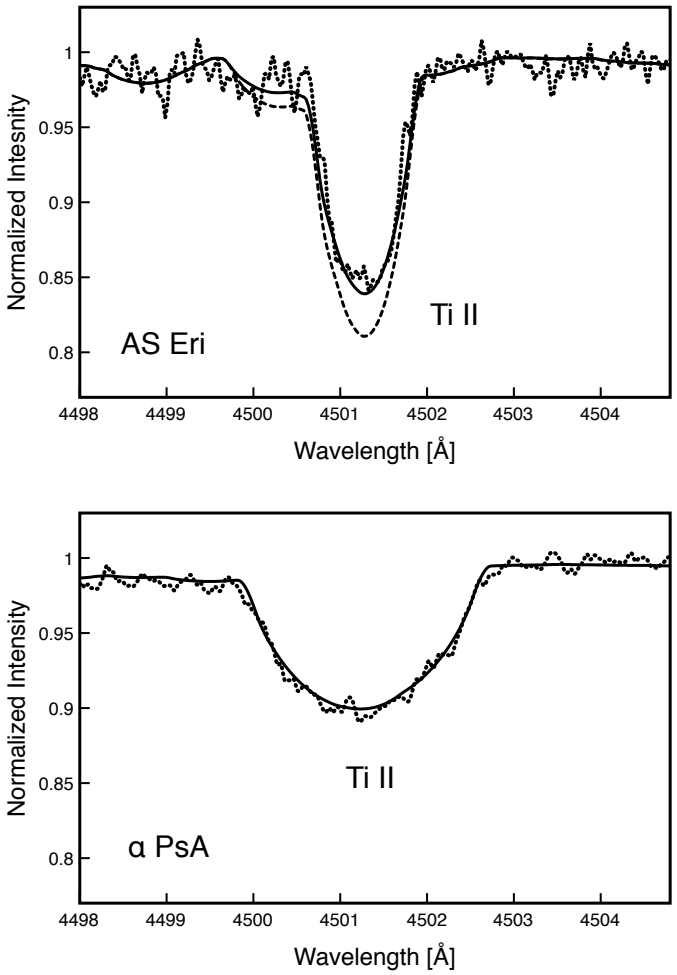

Fig. 7. Spectral synthesis analysis of Ti II feature near 4501 Å. Obseved spectra and final fit solutions are shown by dots and solid lines, respectively. Resulting abundances of Ti obtained from this spectral segment are log N(Ti) = 4.87 and 5.37 in AS Eri-p (DATA2) and α PsA, respectively. The dashed line for AS Eri-p represents a simulation for the case of log N(Ti) = 5.37.

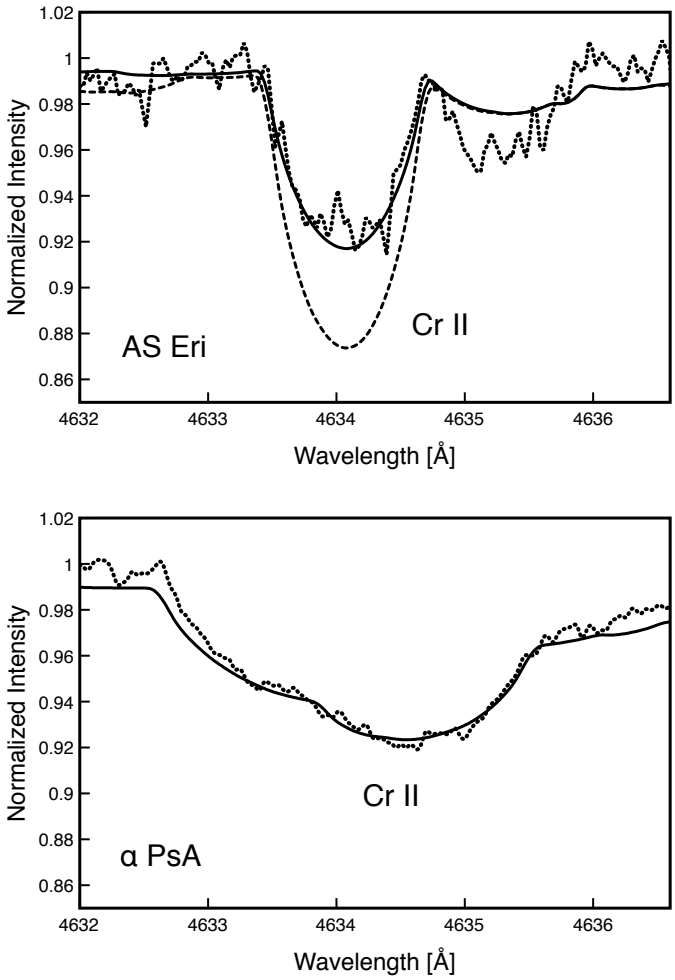

Fig. 8. Spectral synthesis analysis of Cr II feature near 4634 Å. Obseved spectra and final fit solutions are shown by dots and solid lines, respectively. Resulting abundances of Cr obtained from this spectral segment are log $N(\mathrm{Cr}) = 5.74$ and 6.20 in AS Eri-p (DATA2) and α PsA, respectively. The dashed line for AS Eri-p represents a simulation for the case of log $N(\mathrm{Cr}) = 6.20$.